Journal of Applied Physics

A hybrid coupler for directing quantum light emission with high radiative Purcell enhancement to a dielectric metasurface lens

Cite as: J. Appl. Phys. **130**, 163103 (2021); https://doi.org/10.1063/5.0059012
Submitted: 25 June 2021 • Accepted: 03 October 2021 • Published Online: 26 October 2021

Frank Yang, Pankaj Kumar Jha, Hamidreza Akbari, et al.

Journal of Applied Physics ARTICLE scitation.org/journal/jap

A hybrid coupler for directing quantum light emission with high radiative Purcell enhancement to a dielectric metasurface lens

Cite as: J. Appl. Phys. **130**, 163103 (2021); doi: 10.1063/5.0059012
Submitted: 25 June 2021 · Accepted: 3 October 2021 ·
Published Online: 26 October 2021

Frank Yang,[1,2] Pankaj Kumar Jha,[2] Hamidreza Akbari,[2] Haley C. Bauser,[2] and Harry A. Atwater[2,a)]

AFFILIATIONS

[1]Department of Electrical and Computer Engineering, Rice University, Houston, Texas 77005, USA
[2]Thomas J. Watson Laboratory of Applied Physics and Materials Science, California Institute of Technology, Pasadena, California 91125, USA

[a)]**Author to whom correspondence should be addressed:** haa@caltech.edu

ABSTRACT

Quantum photonic technologies such as quantum sensing, metrology, and simulation could be transformatively enabled by the availability of integrated single photon sources with high radiative rates and photon collection efficiencies. We address these challenges for quantum emitters formed from color center defect sites such as those in hexagonal boron nitride, which are promising candidates as single photon sources due to their bright, stable, polarized, and room temperature emission. We report design of a nanophotonic coupler from color center quantum emitters to a dielectric metasurface lens. The coupler is comprised of a hybrid plasmonic–dielectric resonator that achieves a large radiative Purcell enhancement and partial control of far-field radiation. We report radiative Purcell factors up to 285 and photon collection efficiencies up to 89% for a lossless metasurface, applying a continuous hyperboloidal phase-front. Our hybrid plasmonic–dielectric coupler interfacing two nanophotonic elements is a compound optical element, analogous to those found in microscope objective lenses, which combine multiple optical functions into a single component for improved performance.

INTRODUCTION

Single photon sources are physical systems capable of emitting photons on demand and are applicable for quantum sensing, cryptography, metrology, and simulation.[1–3] An ideal single photon source is an emitter triggered by an optical or electrical excitation that emits a single photon of controlled frequency, wavevector, and polarization in response to a control excitation. Many material systems have been shown to exhibit single photon emission, including trapped ions,[4] color center defects in wide bandgap materials such as diamond[5] and silicon carbide,[6] quantum dots,[7] organic molecules,[8] and carbon nanotubes.[9] Quantum emitters formed from color center defects in hexagonal boron nitride (*h*BN), a wide bandgap Van der Waals material, are one promising material platform exhibiting single photon emission. Hexagonal boron nitride point defects have been reported to exhibit room temperature single photon emission that is polarized and photostable. They also have record high brightness, narrow emission spectra, and high intensity of the zero-phonon line with respect to phonon sidebands.[10,11] Recent experiments have shown that the axial position and the 3D dipole orientation of *h*BN quantum emitters can be accurately measured.[12] Furthermore, some of these quantum emitters have very strong out-of-plane dipole orientation, which is highly desirable for tuning emission wavelength using external electric fields.[13–15]

Outstanding challenges in the design of efficient single photon sources include achieving a useful high radiative rate, high photon extraction efficiency, and also control of far-field radiation. High radiative rates are required for high frequency operation, and efficient photon extraction is required for deterministic generation of photons, which is important for many quantum photonic technologies such as secure quantum communication and photonic quantum computation. Currently, bulky optical components, coupled by free-space light propagation, are needed to efficiently capture photon emission from quantum emitters. These preclude design of compact, integrated single photon sources. Prior works

have sought to address these challenges by coupling point defects with nanoantennas,[16–20,21] waveguides,[22,23] or grating structures.[24] Solid immersion lenses have also yielded near unity photon collection efficiency,[25,26] and in one recent work, a metasurface was used to image diamond NV centers.[27] Metasurfaces have also been used to generate and control non-classical light and facilitate quantum interference[28–32] and entanglement.[32,33]

In this work, we design a nanophotonic coupler comprised of a hybrid plasmonic–dielectric resonator that couples emitted photons from quantum emitters to a dielectric metasurface lens. The device achieves a high radiative Purcell factor, collection efficiency, and degree of control over far-field radiation. First, quantum emitters in *h*BN are coupled to hybrid plasmonic–dielectric resonators (Fig. 1). Similar plasmonic nanogap resonators have been explored for plasmonic lasing[34] and large Purcell enhancement.[35] High field confinement results in large radiative Purcell factor, and resonators efficiently outcouple photons to free space.

Previous reports have demonstrated coupling *h*BN emitters to plasmonic resonances, including single nanoantennas,[36] gap dimer modes,[37] and lattice modes.[38] Simulations for single nanoantennas indicate radiative Purcell factors ∼10,[36] while simulations of gap dimer modes report total Purcell factors up to 1200.[37] However, in this case, radiative quantum efficiency is not considered. In all these cases, the reported experimental values for emission intensity enhancement do not exceed one order of magnitude. Designs with dielectric materials such as microcavities[39] and monolithic photonic crystal cavities[40] report Purcell factors of ∼4 and ∼15 in experiments. While Purcell enhancements reported in our work are obtained via simulations (and would likely represent an upper bound for experimentally achievable values), the hybrid design offers some unique benefits. Our design uniquely combines advantages of plasmonic and dielectric couplers. Plasmonic designs generally achieve high local fields and Purcell enhancements on the nanometer scale at the cost of absorptive losses. Meanwhile, designs using dielectric materials, such as microcavities and photonic crystal cavities, suffer fewer absorption losses but at the cost of light confinement. The hybrid coupler presented here achieves both the goals of low loss and high light confinement.

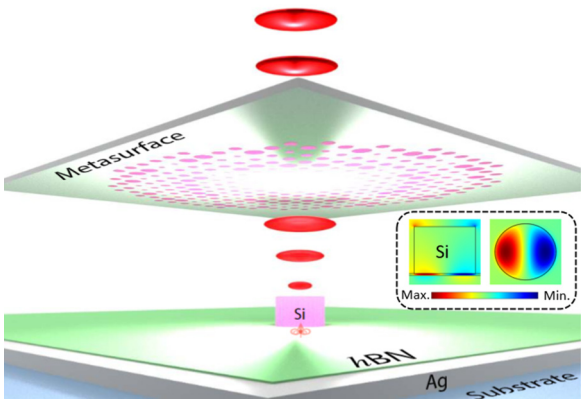

FIG. 1. Overview of device design. *Z*-oriented dipole sits in a thin *h*BN layer between a silver substrate and cylindrical silicon antenna, resulting in high radiative Purcell enhancement. The antenna's output radiation is efficiently collected and collimated by a α-SiC:H dielectric metasurface on the silica substrate. Inset: Imag(Ez) mode profile of silicon antenna.

The second component to this work is an efficient dielectric metasurface, which collects and collimates photons emitted from the plasmonic–dielectric resonator (Fig. 1). Metasurfaces are two-dimensional subwavelength arrays of scatterers capable of controlling the amplitude, phase, and polarization of incident light.[41–44] Metasurfaces allow precise control over the phase-front of input light. Individual metasurface scatterers are resonantly excited by input light and induce controllable phase jumps at the surface, which may be used to construct phase gradients. This enables applications such as beam steering[45] and focusing.[46] Efficient transmissive dielectric metasurfaces have been demonstrated at optical wavelengths using materials such as TiO_2 and Si_3N_4.[47,48] In this work, dielectric scatterers are preferable to plasmonic (metal) structures due to lower absorption losses.[48] Additionally, a metasurface is an apt choice for this collector lens because of low linewidths of *h*BN quantum emission.[11] Metasurfaces are generally dispersive, which can be disadvantageous for applications like broadband imaging. On the other hand, single photon emitters in *h*BN only require precise wavefront control at narrowband wavelength, eliminating drawbacks present in general metasurface imaging. The design we present is an important step toward realizing nanoscale and micron-scale integrated single photon sources. Careful design of the near-field and far-field environment of the emitter allows for efficient and bright sources with extreme wavefront control.

COMBINING PURCELL ENHANCEMENT AND META-OPTICS

In order to obtain partial control over quantum emitter far-field radiation patterns and increase their spontaneous emission rates, we carefully designed the optical environment of the emitter. Coupling quantum emitters with plasmonic–dielectric antennas yields partial control over emitter far-field radiation. Coupling also increases the local optical density of states, ultimately increasing the spontaneous emission rate via the Purcell effect. Using finite-difference time-domain simulations (Lumerical), we model an emitter with a *z*-oriented dipole embedded in multilayer *h*BN. Quantum light emission from *h*BN color centers has been observed in several wavelength ranges, ranging from the visible to near-IR, and we select a representative emitter wavelength of 623 nm based on past works.[11,49,50] The *h*BN layer sits on a silver substrate. A cylindrical silicon resonator sits on the *h*BN layer (see S1 in the supplementary material for optical constants). The dielectric nanocylinder and silver substrate support a plasmonic–dielectric resonance offering high field enhancement in the *h*BN layer,[21] as shown in field profiles in Fig. 1. Mode profiles are obtained by exciting the resonator with an x-polarized plane wave and recording field in the center of the *h*BN spacer layer. Large electric fields correspond to increased local density of states and enhancement of the spontaneous emission rate.

The *h*BN layer is 4 nm thick.[50] The choice of multilayer *h*BN is made because of past works achieving similar thicknesses of *h*BN by exfoliation[18] and chemical vapor deposition.[50] Also, multilayer *h*BN has been shown to exhibit color centers with greater spectral

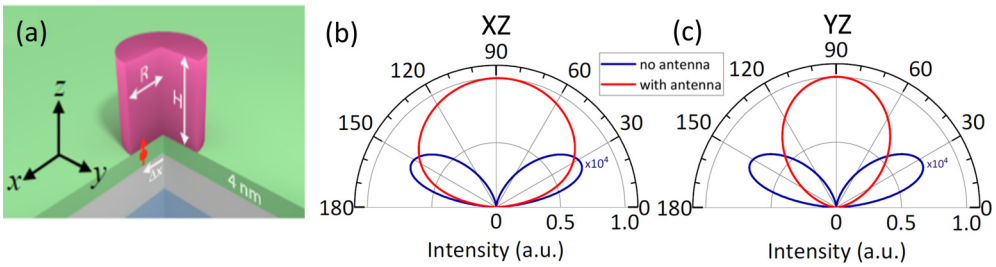

FIG. 2. Antenna-emitter coupled system. (a) Z-oriented dipole sits in a thin *h*BN layer between a silver substrate and cylindrical silicon antenna, resulting in high radiative Purcell enhancement. (b) and (c) Far-field radiation plots of output antenna radiation of the antenna-emitter system (red) and *h*BN emitter on the silver substrate (blue).

stability as compared to monolayer or few-layer flakes.[50] Figure 2(a) gives a schematic of the plasmonic–dielectric resonator. Hybrid plasmonic–dielectric modes can be conceptualized as surface plasmons reflecting off the boundaries of the dielectric nanocylinder. They are described by indices (n and m), where n represents radial and m represents azimuthal field variation. We designed a silicon nanocylinder such that the (1, 1) mode occurs at the design wavelength (Fig. 1, inset). We optimized the geometry of the nanocylinder in full-wave simulations (Lumerical) by exciting the hybrid resonator using a total-field scattered-field source and sweeping over parameters. For a wavelength of 623 nm, this results in a silicon nanocylinder with h = 100 nm and R = 46 nm. The *z*-oriented dipole is placed at Δx = 34 nm to maximize the overlap of the dipole with electric fields, which increases Purcell enhancement. Purcell factor is computed using full-wave simulation and the Lumerical built-in function with a dipole source embedded in *h*BN. The plasmonic–dielectric resonator yields partial control over the far-field radiation pattern of the dipole, as shown in Figs. 2(b) and 2(c). With no silicon nanocylinder, a *z*-dipole embedded in *h*BN on a silver substrate exhibits two symmetric radiation lobes; and radiation is highly non-directional. The addition of the silicon nanocylinder results in a far-field pattern containing a single lobe. This result is important because it allows for efficient collection of photons using metasurfaces. Near-to-far-field transformations are performed using an open source software based on Lorentz reciprocity.[51] The plasmonic–dielectric resonator enhances the spontaneous emission rate of the *h*BN emitter. This effect is quantified by the Purcell factor, which is the ratio between emitted power in an engineered environment (γ_{tot}) and emitted power in a homogeneous environment (γ_0). Equation (1) gives an expression for the Purcell factor. P_0 is the power radiated by a dipole in homogeneous media, μ is the dipole moment, and E is the electric field,

$$\frac{\gamma_{tot}}{\gamma_0} = \frac{\omega}{2P_0} Im\{\mu^* \cdot E\}. \tag{1}$$

The Purcell factor depends on the imaginary part of the dot product of the dipole moment and field. The hybrid plasmonic–dielectric resonance exhibits high enhancements in the z-component of electric field, which is highly confined to the *h*BN layer. This high field enhancement is the basis of the design and also the reason for the selection of a z-oriented dipole. It is important to note that Purcell enhancement in this configuration depends strongly on *h*BN gap thickness (<10 nm) with thicker gaps resulting in lower field enhancement and Purcell factor.[21] Figures 3(a) and 3(b) give a spatial mapping of Purcell factor for a z-oriented dipole situated in the *h*BN layer. Maximum Purcell factor of 700 occurs at Δx = 34 nm, coinciding with the highest field intensities of the (1,1) mode (see Fig. 1, inset). Because the system is not lossless, the Purcell enhancement has a contribution from increased decay to free-space radiative channels (γ_{rad}), surface plasmon polaritons (γ_{SPP}), and non-radiative channels (γ_{abs}), given by Eq. (2). Silver is one of the least lossy metals in the visible. As a result, the resonator structure efficiently launches surface plasmon polaritons when excited by dipole radiation. Sources of absorption include silver and silicon, which has a small but finite imaginary part of refractive index at the design wavelength (623 nm). For reference, the antenna simulation design is repeated while replacing the silver substrate with a perfect electrical conductor in S2 in the supplementary material. As shown in Fig. 3(c), the radiative component of Purcell factor, $\frac{\gamma_{rad}}{\gamma_0}$, exhibits a maximum of 285 at the design wavelength,

$$\gamma_{tot} = \gamma_{rad} + \gamma_{SPP} + \gamma_{abs}. \tag{2}$$

We seek to maximize the radiative component of Purcell factor and minimize absorption losses. Our figure of merit is the radiative quantum efficiency, in which we consider the rate of photon generation. This is given by Eq. (3). Quantum efficiency is plotted in Fig. 3(d). For this system, the radiative quantum efficiency reaches a maximum of 0.4 at the design wavelength,

$$QE = \frac{\gamma_{rad}}{\gamma_{tot}}. \tag{3}$$

The plasmonic–dielectric resonator has several functions. It increases spontaneous emission rate and outcouples photons to free space by effectively transforming the radiation pattern of a vertical (z-oriented) dipole to that of a horizontal (x-oriented) dipole. The resonator configuration depends heavily on the vertical component of the dipole emitter, as shown in Fig. 3(e). Radiative Purcell factor drops dramatically as the polar angle Θ is increased

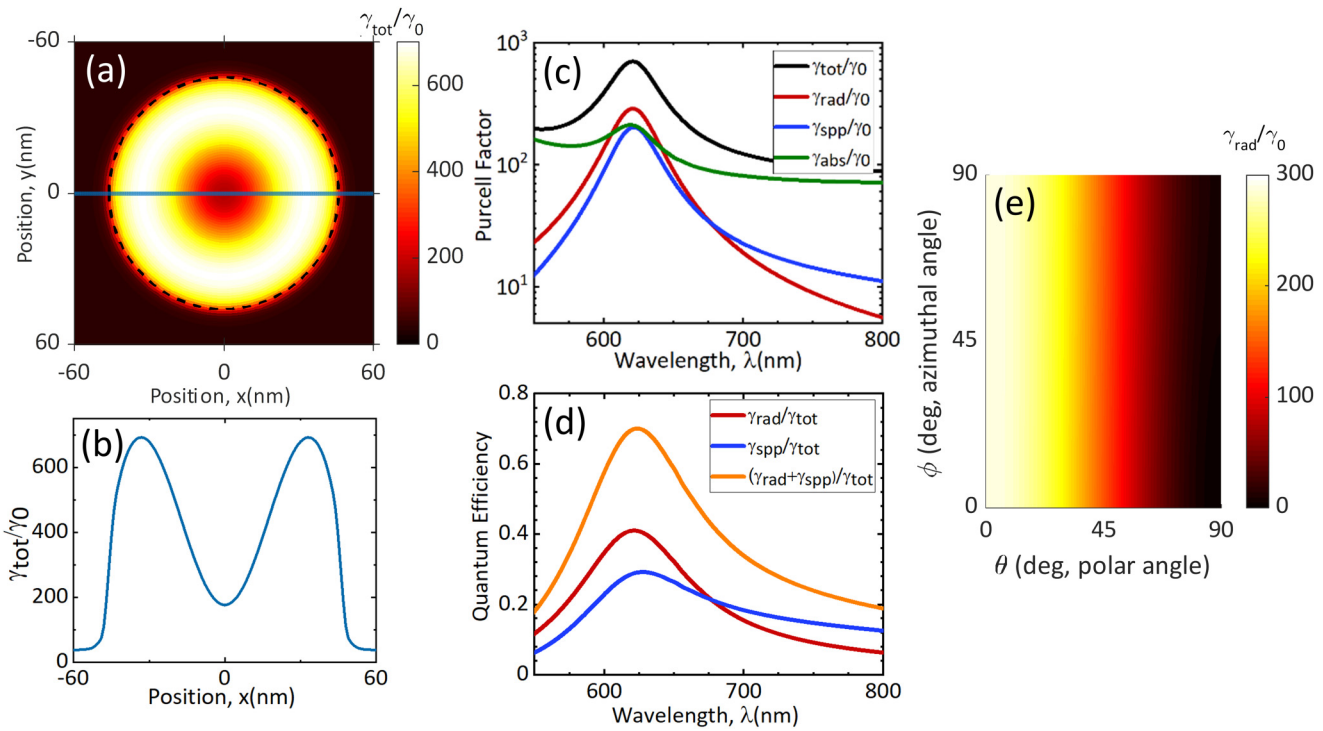

FIG. 3. Purcell enhancement induced by silicon antenna. (a) Spatial mapping of Purcell enhancement for silicon antenna of height 100 nm and radius 46 nm. (b) Plot of Purcell enhancement vs dipole position showing a maximum for a dipole at radius 34 nm. (c) Purcell enhancement vs wavelength (d) and radiative quantum efficiency vs wavelength for dipole at radius 34 nm. (e) Radiative Purcell factor vs dipole orientation showing strong dependence on the z-component of dipole.

from 0. Photons coupled to free space are collected and collimated with a dielectric metasurface. Metasurfaces are composed of arrays of subwavelength scatterers. We choose amorphous silicon carbide (α-SiC:H) cylindrical scatterers[52,53] due to the high index and low absorption of silicon carbide in the visible. Cylindrical symmetry of scatterers ensures that the final device is polarization insensitive. Cylindrical silicon carbide resonators with height = 350 nm are placed in a square lattice of period = 300 nm [Fig. 4(a), inset]. By varying cylinder radius, we find that the full 2π phase needed for metasurface operation is accessible [Fig. 4(a)]. This 2π range is discretized into eight phase values (0, π/4, π/2, …, 7π/4). Optimal cylinder radii are selected to maximize transmission with average transmission of 0.9633. Metasurface building blocks were simulated in Lumerical as follows. Silicon carbide cylinders are placed on quartz and excited using an x-polarized, plane wave input. One period of the square lattice is simulated, and periodic boundary conditions are used. Phase is computed using a two-dimensional Fourier-transform of the electric fields and taking the phase of the

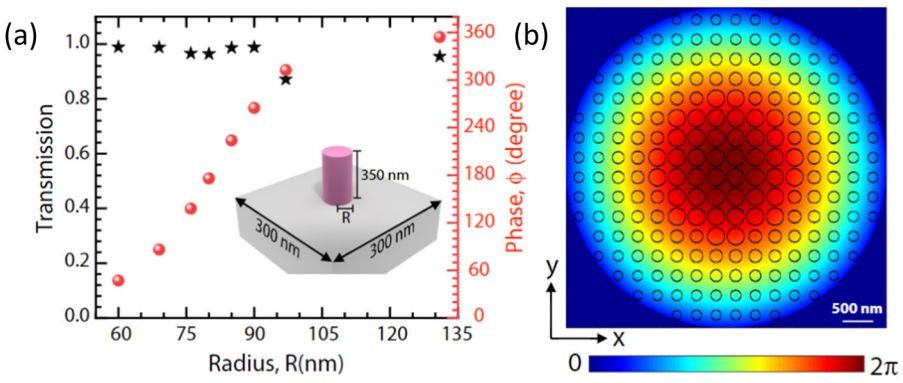

FIG. 4. Metasurface device. (a) Transmission and phase vs phase of (α-SiC:H) metasurface scatterers on a quartz substrate, showing eight selected metasurface resonators. (b) Metasurface phase profile of beam collimator with selected scatterers.

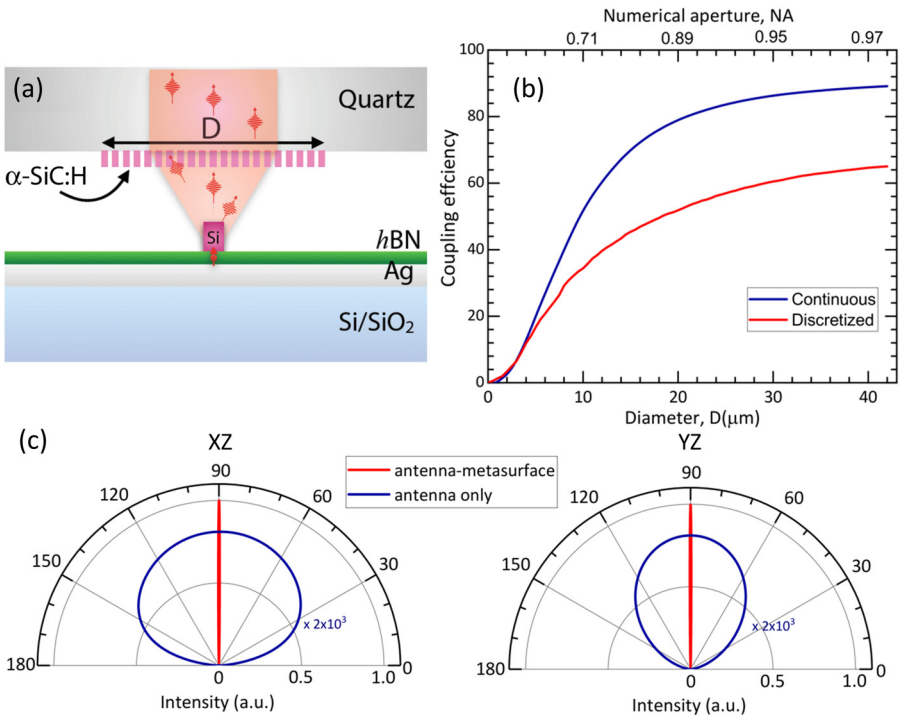

FIG. 5. Antenna-metasurface coupled device. (a) Schematic of antenna-metasurface coupled device, (b) coupling efficiency vs numerical aperture, and (c) far-field radiation pattern for 21 μm metasurface and antenna-emitter system.

propagating wave in the normal direction ($k_x = k_y = 0$ in k-space). Transmission is recorded using power monitors. Detailed analysis of a single metasurface nanocylinder is given in S3 in the supplementary material. We consider that the desired metasurface must collect and collimate radiation from an effective point source which is the silicon nanocylinder antenna. Thus, the hyperboloidal phase profile given in Eq. (4) is appropriate. Here, x and y are the spatial positions of metasurface scatterers, and f is the focal length,

$$\varphi(x, y) = -\frac{2\pi}{\lambda}\left(\sqrt{x^2 + y^2 + f^2} - f\right). \tag{4}$$

We design a device with $f = 5\,\mu$m. A cross-sectional cut of such a metasurface is given in Fig. 4(b) with appropriate α-SiC:H scatterers outlined.

The final device is shown in Fig. 5(a). A circular metasurface with diameter D is placed 5 μm above the silicon nanocylinder antenna on a semi-infinite quartz substrate. Figure 5(b) gives the coupling efficiency of the metasurface as a function of numerical aperture, calculated using the Huygens–Fresnel integral and with full-wave FDTD simulations. Coupling efficiency is defined to be the power of transmitted through the metasurface cross-sectional area 10 μm above the metasurface, normalized to the power coupled to free-space photons from the plasmonic–dielectric resonator. To compute coupling efficiency using the Huygens–Fresnel integral, full-wave simulations are used to obtain fields at the metasurface input. These input fields are imparted with the hyperbolic metalens phase profile, and far fields are calculated according to Eq. (5). Electric field at $\boldsymbol{r}_2 = (x_2, y_2, z_2)$ can be obtained from the field at the $z_1 = 0$ plane. In the expression, $r_0 = \sqrt{(x_2 - x_1)^2 + (y_2 - y_1)^2 + (z_2)^2}$ and $\cos(\theta) = \frac{z_2}{r_0}$,

$$\boldsymbol{E}(\boldsymbol{r}_2, \omega) = -\frac{i}{\lambda}\iint \cos(\theta)\left(1 + \frac{i}{kr_0}\right)\frac{e^{ikr_0}}{r_0}\boldsymbol{E}(x_1, y_1, z_1 = 0)dx_1 dy_1. \tag{5}$$

For high numerical aperture ~0.97, coupling efficiency of 0.89 is achieved with the Huygens–Fresnel calculation, representing the lossless metasurface. Full-wave simulation yields maximum coupling efficiency of 0.65. The decreased performance in full-wave simulations can be attributed to sources of loss such as the finite pixel size of each metasurface scatterer and the deviation from phase response of each scatterer obtained for normal incidence due to high numerical aperture (NA) of the device. In contrast to the Huygens–Fresnel calculation, which applies a continuous phase-front, the full-wave metasurface applies phase at each scatterer. The high NA of the metasurface results in varying optical response from each α-SiC:H resonator as the incident angle of input light is increased. Metasurface elements on the edge of the device are no longer excited by normally incident light. Figure 5(c) gives a visualization for the beam collimation after photons have passed the metasurface. As evidenced in the far-field radiation patterns, the metasurface redirects incident photons into a tightly collimated beam, which will be useful for quantum photonic applications.

CONCLUSION AND OUTLOOK

In summary, we have employed nanophotonic design to manipulate single photon emission, building a device with high radiative Purcell enhancement, high photon collection efficiency, and strongly directional emission. We show that a hybrid plasmonic–dielectric resonator antenna can be coupled with an *h*BN quantum emitter to reach radiative Purcell factors up to 285. However, the radiation from such nanoscale antennas is not highly directional. By interfacing the nanoscale antenna with a dielectric metasurface, we efficiently collect and control output radiation, resulting in highly directional and efficient emission. For a lossless metasurface, we report photon collection efficiences up to 89%. When combined with the radiative quantum efficiency of 0.4, the complete system efficiency is 35.6%. With the addition of sources of loss such as finite pixel discretization and angular response of scatterers, photon collection efficiency reaches 65% (full-wave simulations), corresponding to complete system efficiency of 26%. Future works will investigate designs to increase radiative quantum efficiency. One avenue is to investigate substitutes for the metal back-reflector to prevent the coupling of emission to surface plasmons (rather than free-space photons). Another is to investigate other dielectrics for the nanocylinder antenna because of finite absorption in the silicon antenna.

Experimental demonstration of our proposed designs is another future direction for this work. Device fabrication can be completed with established techniques. The metasurface can be fabricated by a top-down approach.[54] First, amorphous silicon carbide can be deposited by plasma-enhanced chemical vapor deposition.[52] Then, established electron-beam-lithography techniques can be used to pattern the film, followed by deep reactive-ion-etching to define metasurface scatterers. To fabricate and position silicon nanoantennas, approaches such as AFM tip manipulation of nanoparticles are a viable option.[37]

This device is an important step forward for integrated quantum optical technologies. It is also not limited to quantum applications and could be applied to build novel light sources in other material systems. For example, interlayer excitons in van der Waals heterostructures have a strong *z*-component of electric dipole.[55] Coupling such excitons with similar resonator designs could yield light sources with high radiative Purcell factor and controllable far-field radiation.

SUPPLEMENTARY MATERIAL

See the supplementary material for the details regarding optical constants used in simulations (S1), analysis of an emitter coupled to a hybrid resonator using a perfect electrical conductor substrate (S2), and analysis of a single α-SiC:H metasurface nanocylinder (S3).

ACKNOWLEDGMENTS

This work was supported by the "Photonics at Thermodynamic Limits" Energy Frontier Research Center funded by the U.S. Department of Energy, Office of Science, Office of Basic Energy Sciences under Award Number DE-SC0019140. This work was also supported by the U.S. Department of Defense, U.S. Air Force, Air Mobility Command, Air Force Office of Scientific Research (AFOSR) under Award Number FA2386-18-1-4095.

AUTHOR DECLARATIONS

Conflict of Interest

The authors have no conflict to disclose.

Author Contributions

F.Y. and P.K.J. contributed equally to this work.

DATA AVAILABILITY

The data that support the findings of this study are available from the corresponding author upon reasonable request.

REFERENCES

[1]J. L. O'Brien, A. Furusawa, and J. Vuckovic, "Photonic quantum technologies," Nat. Photonics **3**, 687–695 (2009).
[2]M. Fox, *Quantum Optics: An Introduction*, Oxford Master Series in Physics (Oxford University Press, Oxford, 2006).
[3]M. Toth and I. Aharonovich, "Single photon sources in atomically thin materials," Annu. Rev. Phys. Chem. **70**, 123–142 (2019).
[4]M. Keller, B. Lange, K. Hayasaka, W. Lange, and H. Walther, "Continuous generation of single photons with controlled waveform in an ion-trap cavity system," Nature **431**, 1075–1078 (2004).
[5]N. Mizuochi, T. Makino, H. Kato, D. Takeuchi, M. Ogura, H. Okushi, M. Nothaft, P. Neumann, A. Gali, F. Jelezko, J. Wrachtrup, and S. Yamasaki, "Electrically driven single-photon source at room temperature in diamond," Nat. Photonics **6**, 299–303 (2012).
[6]D. D. Awschalom, R. Hanson, J. Wrachtrup, and B. B. Zhou, "Quantum technologies with optically interfaced solid-state spins," Nat. Photonics **12**, 516–527 (2018).
[7]P. Senellart, G. Solomon, and A. White, "High-performance semiconductor quantum-dot single-photon sources," Nat. Nanotechnol. **12**, 1026–1039 (2017).
[8]C. Browne, T. Farrow, O. C. O. Dahlsten, R. A. Taylor, and V. Vlatko, "Organic molecule fluorescence as an experimental test-bed for quantum jumps in thermodynamics," Proc. R. Soc. A **473**, 20170099 (2017).
[9]A. Ishii, X. He, N. F. Hartmann, H. Machiya, H. Htoon, S. K. Doorn, and Y. K. Kato, "Enhanced single-photon emission from carbon-nanotube dopant states coupled to silicon microcavities," Nano Lett. **18**, 3873–3878 (2018).
[10]I. Aharonovich, D. Englund, and M. Toth, "Solid-state single-photon emitters," Nat. Photonics **10**, 631–641 (2016).
[11]T. T. Tran, K. Bray, M. J. Ford, M. Toth, and I. Aharonovich, "Quantum emission from hexagonal boron nitride monolayers," Nat. Nanotechnol. **11**, 37–41 (2016).
[12]P. K. Jha, H. Akbari, Y. Kim, S. Biswas, and H. A. Atwater, "Nanoscale axial position and orientation measurement of hexagonal boron nitride quantum emitters using a tunable nanophotonic environment," Nanotechnology **33**(1), 015001 (2021).
[13]G. Noh, D. Choi, J.-H. Kim, D.-G. Im, Y.-H. Kim, H. Seo, and J. Lee, "Stark tuning of single-photon emitters in hexagonal boron nitride," Nano Lett. **18**, 4710–4715 (2018).
[14]N. Nikolay, N. Mendelson, N. Sadzak, F. Bohm, T. T. Tran, B. Sontheimer, I. Aharonovich, and O. Benson, "Very large and reversible Stark-shift tuning of single emitters in layered hexagonal boron nitride," Phys. Rev. Appl. **11**, 041001 (2019).
[15]Y. Xia, Q. Li, J. Kim, W. Bao, C. Gong, S. Yang, Y. Wang, and X. Zhang, "Room-temperature giant Stark effect of single photon emitter in van der Waals material," Nano Lett. **19**, 7100–7105 (2019).

[16]G. M. Akselrod, C. Argyropoulos, T. B. Hoang, C. Ciraci, C. Fang, J. Huang, D. R. Smith, and M. H. Mikkelsen, "Probing the mechanisms of large Purcell enhancement in plasmonic nanoantennas," Nat. Photonics **8**, 835–840 (2014).
[17]A. Karamlou, M. E. Trusheim, and D. Englund, "Metal-dielectric antennas for efficient photon collection from diamond color centers," Opt. Express **26**, 3341–3352 (2018).
[18]N. Palombo Blascetta, M. Liebel, X. Lu, T. Taniguchi, K. Watanabe, D. K. Efetov, and N. F. van Hulst, "Nanoscale imaging and control of hexagonal boron nitride single photon emitters by a resonant nanoantenna," Nano Lett. **20**, 1992–1999 (2020).
[19]X. Li, R. A. Scully, K. Shayan, Y. Luo, and S. Strauf, "Near-unity light collection efficiency from quantum emitters in boron nitride by coupling to metallo-dielectric antennas," ACS Nano **13**, 6992–6997 (2019).
[20]S. K. H. Andersen, S. Bogdanov, O. Makarova, Y. Xuan, M. Y. Shalaginov, A. Boltasseva, S. I. Bozhevolnyi, and V. M. Shalaev, "Hybrid plasmonic bullseye antennas for efficient photon collection," ACS Photonics **5**, 692–698 (2018).
[21]Y. Yang, O. D. Miller, T. Christensen, J. D. Joannopoulos, and M. Soljacic, "Low-loss plasmonic dielectric nanoresonators," Nano Lett. **17**, 3238–3245 (2017).
[22]R. N. Patel, T. Schroder, N. Wan, L. Li, S. L. Mouradian, E. H. Chen, and D. R. Englund, "Efficient photon coupling from a diamond nitrogen vacancy center by integration with silica fiber," Light Sci. Appl. **5**, e16032 (2016).
[23]D. Le Sage, L. M. Pham, N. Bar-Gill, C. Belthangady, M. D. Lukin, A. Yacoby, and R. L. Walsworth, "Efficient photon detection from color centers in a diamond optical waveguide," Phys. Rev. B **85**, 121202 (2012).
[24]L. Li, E. H. Chen, J. Zheng, S. L. Mouradian, F. Dolde, T. Schroder, S. Karaveli, M. L. Markham, D. J. Twitchen, and D. Englund, "Efficient photon collection from a nitrogen vacancy center in a circular bullseye grating," Nano Lett. **15**, 1493–1497 (2015).
[25]X.-W. Chen, S. Gotzinger, and V. Sandoghdar, "99% efficiency in collecting photons from a single emitter," Opt. Lett. **36**, 3545–3547 (2011).
[26]D. Riedel, D. Rohner, M. Ganzhorn, T. Kaldewey, P. Appel, E. Neu, R. J. Warburton, and P. Maletinsky, "Low-loss broadband antenna for efficient photon collection from a coherent spin in diamond," Phys. Rev. Appl. **2**, 064011 (2014).
[27]T.-Y. Huang, R. R. Grote, S. A. Mann, D. A. Hopper, A. L. Exarhos, G. G. Lopez, G. R. Kaighn, E. C. Garnett, and L. C. Bassett, "A monolithic immersion metalens for imaging solid-state quantum emitters," Nat. Commun. **10**, 1–8 (2019).
[28]P. K. Jha, X. Ni, C. Wu, Y. Wang, and X. Zhang, "Metasurface-enabled remote quantum interference," Phys. Rev. Lett. **115**, 025501 (2015).
[29]M. Sohoni, P. K. Jha, M. Nalabothula, and A. Kumar, "Interlayer exciton valleytronics in bilayer heterostructures interfaced with a phase gradient metasurface," Appl. Phys. Lett. **117**, 121101 (2020).
[30]X. Ren, P. K. Jha, Y. Wang, and X. Zhang, "Nonconventional metasurfaces: From non-Hermitian coupling, quantum interactions, to skin cloak," Nanophotonics **7**, 1233–1243 (2018).
[31]P. K. Jha, N. Shitrit, X. Ren, Y. Wang, and X. Zhang, "Spontaneous exciton valley coherence in transition metal dichalcogenide monolayers interfaced with an anisotropic metasurface," Phys. Rev. Lett. **121**, 116102 (2018).
[32]A. S. Solntsev, G. S. Agarwal, and Y. S. Kivshar, "Metasurfaces for quantum photonics," Nat. Photonics **15**, 327–336 (2021).
[33]P. K. Jha, N. Shitrit, J. Kim, X. Ren, Y. Wang, and X. Zhang, "Metasurface-mediated quantum entanglement," ACS Photonics **5**, 971–976 (2018).
[34]R. F. Oulton, V. J. Sorger, T. Zentgraf, R.-M. Ma, C. Gladden, L. Dai, G. Bartal, and X. Zhang, "Plasmon lasers at deep subwavelength scale," Nature **461**, 629–632 (2009).
[35]J. J. Baumberg, J. Aizpurua, M. H. Mikkelsen, and D. R. Smith, "Extreme nanophotonics from ultrathin metallic gaps," Nat. Mater. **18**, 668–678 (2019).
[36]A. Singh, P. M. de Roque, G. Calbris, J. T. Hugall, and N. F. van Hulst, "Nanoscale mapping and control of antenna-coupling strength for bright single photon sources," Nano Lett. **18**, 2538–2544 (2018).
[37]M. Nguyen, S. Kim, T. T. Tran, Z.-Q. Xu, M. Kianinia, M. Toth, and I. Aharonovich, "Nanoassembly of quantum emitters in hexagonal boron nitride and gold nanospheres," Nanoscale **10**, 2267–2274 (2018).
[38]T. T. Tran, D. Wang, Z.-Q. Xu, A. Yang, M. Toth, T. W. Odom, and I. Aharonovich, "Deterministic coupling of quantum emitters in 2D materials to plasmonic nanocavity arrays," Nano Lett. **17**, 2634–2639 (2017).
[39]T. Vogl, R. Lecamwasam, B. C. Buchler, Y. Lu, and P. K. Lam, "Compact cavity-enhanced single-photon generation with hexagonal boron nitride," ACS Photonics **6**, 1955–1962 (2019).
[40]J. E. Fröch, C. Li, Y. Chen, M. Toth, M. Kianinia, S. Kim, and I. Aharonovich, "Purcell enhancement of a cavity-coupled emitter in hexagonal boron nitride," arXiv:2108.05268 (2021).
[41]N. Yu and F. Capasso, "Flat optics with designer metasurfaces," Nat. Mater. **13**, 139–150 (2014).
[42]A. V. Kildishev, A. Boltasseva, and V. M. Shalaev, "Planar photonics with metasurfaces," Science **339**, 1232009 (2013).
[43]S. M. Kamali, E. Arbabi, A. Arbabi, and A. Faraon, "A review of dielectric optical metasurfaces for wavefront control," Nanophotonics **7**, 1041–1068 (2018).
[44]F. Ding, A. Pors, and S. I. Bozhevolnyi, "Gradient metasurfaces: A review of fundamentals and applications," Rep. Prog. Phys. **81**, 026401 (2017).
[45]Y.-W. Huang, H. W. H. Lee, R. Sokhoyan, R. A. Pala, K. Thyagarajan, S. Han, D. P. Tsai, and H. A. Atwater, "Gate-tunable conducting oxide metasurfaces," Nano Lett. **16**, 5319–5325 (2016).
[46]M. Khorasaninejad, W. T. Chen, R. C. Devlin, J. Oh, A. Y. Zhu, and F. Capasso, "Metalenses at visible wavelengths: Diffraction-limited focusing and subwavelength resolution imaging," Science **352**, 1190–1194 (2016).
[47]A. Zhan, S. Colburn, R. Trivedi, T. K. Fryett, C. M. Dodson, and A. Majumdar, "Low-contrast dielectric metasurface optics," ACS Photonics **3**, 209–214 (2016).
[48]P. Genevet, F. Capasso, F. Aieta, M. Khorasaninejad, and R. Devlin, "Recent advances in planar optics: From plasmonic to dielectric metasurfaces," Optica **4**, 139–152 (2017).
[49]A. Sajid, M. J. Ford, and J. R. Reimers, "Single-photon emitters in hexagonal boron nitride: A review of progress," Rep. Prog. Phys. **83**, 044501 (2020).
[50]H. Akbari, W.-H. Lin, B. Vest, P. K. Jha, and H. A. Atwater, "Temperature-dependent spectral emission of hexagonal boron nitride quantum emitters on conductive and dielectric substrates," Phys. Rev. Appl. **15**, 014036 (2021).
[51]J. Yang, J.-P. Hugonin, and P. Lalanne, "Near-to-far field transformations for radiative and guided waves," ACS Photonics **3**, 395–402 (2016).
[52]M. Boccard and Z. C. Holman, "Amorphous silicon carbide passivating layers for crystalline-silicon-carbide-based heterojunction solar cells," J. Appl. Phys. **118**, 065704 (2015).
[53]H. C. Bauser, C. R. Bukowsky, M. Phelan, W. Weigand, D. R. Needell, Z. C. Holman, and H. A. Atwater, "Photonic crystal waveguides for >90% light trapping efficiency in luminescent solar concentrators," ACS Photonics **7**, 2122–2131 (2020).
[54]R. C. Ng, J. C. Garcia, J. R. Greer, and K. T. Fountaine, "Independent, narrow-band, near-IR spectral filters via guided mode resonances in ultrathin a-Si nano-pillar arrays," ACS Photonics **6**, 265–271 (2019).
[55]J. S. Ross, P. Rivera, J. Schaibley, E. Lee-Wong, H. Yu, T. Taniguchi, K. Watanabe, J. Yan, D. Mandrus, D. Cobden, W. Yao, and X. Xu, "Interlayer exciton optoelectronics in a 2D heterostructure p-n junction," Nano Lett. **17**, 638–643 (2017).